Ultra-Specific Zeptomole MicroRNA Detection by Plasmonic Nanowire Interstice Sensor with Bi-Temperature Hybridization

Taejoon Kang, Hongki Kim, Jeong Min Lee, Hyoban Lee, Yun-Seok Choi, Gyeongwon Kang, Min-Kyo Seo, Bong Hyun Chung, Yongwon Jung,* and Bongsoo Kim**

***M**icroRNAs (miRNAs) are emerging new biomarkers for many human diseases. To fully employ miRNAs as biomarkers for clinical diagnosis, it is most desirable to accurately determine the expression patterns of miRNAs. The optimum miRNA profiling method would feature 1) highest sensitivity with a wide dynamic range for accurate expression patterns, 2) supreme specificity to discriminate single nucleotide polymorphisms (SNPs), and 3) simple sensing processes to minimize measurement variation. Here, an ultra-specific detection method of miRNAs with zeptomole sensitivity is reported by applying bi-temperature hybridizations on single-crystalline plasmonic nanowire interstice (PNI) sensors. This method shows near-perfect accuracy of SNPs and a very low detection limit of 100 aM (50 zeptomole) without any amplification or labeling steps. Furthermore, multiplex sensing capability and wide dynamic ranges (100 aM–100 pM) of this method allows reliable observation of the expression patterns of miRNAs extracted from human tissues. The PNI sensor offers combination of ultra-specificity and zeptomole sensitivity while requiring two steps of hybridization between short oligonucleotides, which could present the best set of features for optimum miRNA sensing method.*

1. Introduction

MicroRNAs (miRNAs) are short and single-stranded RNAs that regulate major portion of gene expression.[1–3] The expression patterns of miRNAs in the tissue and blood samples of patients are often closely associated with disease types and also disease stages, hinting certain miRNAs for compelling diagnostic markers.[4–10] To fully employ miRNAs as biomarkers for diagnosis and prognosis in clinical processes, it is most desirable to accurately determine the expression patterns of miRNAs in human samples. A major challenge in miRNA detection has been to overcome inconsistent measurement results, caused by low specificities and complicated sensing procedures.[11,12] The optimum profiling method of miRNA would feature 1) highest sensitivity with a wide dynamic range for accurate expression patterns, 2) supreme specificity to discriminate even singly mismatched short miRNAs, avoiding false measurements, and 3) simplified processing steps to minimize measurement variation.

While polymerase chain reaction (PCR) assays and microarrays have been most widely used for the detection of miRNA, these methods often suffer from error-prone amplification and cross-hybridization because of aberrantly short

Dr. T. Kang, Dr. B. H. Chung
BioNanotechnology Research Center
and BioNano Health Guard Research Center
KRIBB 305–806, Korea
E-mail: chungbh@kribb.re.kr
H. Kim, Dr. J. M. Lee, Dr. H. Lee, G. Kang, Prof. Y. Jung, Prof. B. Kim
Department of Chemistry
KAIST 305–701, Korea
E-mail: ywjung@kaist.ac.kr; bongsoo@kaist.ac.kr
Y.-S. Choi, Prof. M.-K. Seo
Department of Physics
KAIST 305–701, Korea

DOI: 10.1002/smll.201400164

NANO MICRO small

sequences of miRNAs.[13,14] Recently, utilizing nanostructures for diverse sensing techniques substantially improved the miRNA sensing abilities.[15–27] For examples, Dorvel et al. reported Si nanowire (NW)-based miRNA sensor with a detection limit of 1 fM.[18] Tian et al. demonstrated interference-free detection of miRNAs by using nanopore.[15] Shah et al. designed Ag nanoclusters/DNA probes for fast fluorescent detection of miRNAs in 1 h.[17] Graphene oxide and nanocontainer were also used for intracellular detection of miRNAs.[19,20]

Here, we report ultra-specific detection method of miRNAs with zeptomole sensitivity by applying bi-temperature hybridizations on single-crystalline plasmonic NW interstice (PNI) sensors. This method shows near-perfect accuracy of single nucleotide polymorphism (SNPs) and extremely low detection limit of 100 aM, corresponding to 50 zeptomole in a 500 μL volume for all investigated miRNAs without any chemical or enzymatic reactions. Bringing bi-temperature miRNA hybridizations on atomically smooth Au nanowire surfaces has contributed to the exceptional sensitivity as well as near-perfect discrimination of single base mismatches on miRNAs. Furthermore, wide dynamic ranges (100 aM–100 pM) and multiplex sensing capability of this method enable successful measurements of the expression patterns of miRNAs extracted from human skeletal muscle (SKM) and heart tissues. The present PNI sensor offers combination of ultra-specificity and ultra-sensitivity while requiring only two steps of hybridization between short oligonucleotides, which could present the best set of features for optimum miRNA sensing method. We anticipate that the PNI sensor combined with the bi-temperature hybridization can lead to discovery of novel biomarkers and eventual early diagnosis of corresponding diseases.

2. Results and Discussion

2.1. PNI Sensors Combined with Bi-temperature Hybridization Provide Ultra-specific Detection of miRNAs

Among various kinds of nanostructures, NWs have been employed as superb signal transducers for detection of biological and chemical species because the diameters of NWs are comparable to the size of such species.[28–37] In particular, single-crystalline noble metal NW-based surface-enhanced Raman scattering (SERS) sensors allowed highly sensitive and reproducible detection of diverse biochemical molecules because of their well-defined architecture.[38–44] For the ultra-specific and ultra-sensitive detection of miRNAs, we applied miRNA-specific bi-temperature hybridizations to single-crystalline Au NW surfaces, where short miRNAs can readily crawl into the narrow hot spots of the PNI sensor for effective SERS detection (**Figure 1**a). PNI sensors are fabricated by simply placing a single-crystalline Au NW on a Au film. Au NWs were synthesized on a sapphire substrate by using a vapor transport method.[45] As-synthesized NWs

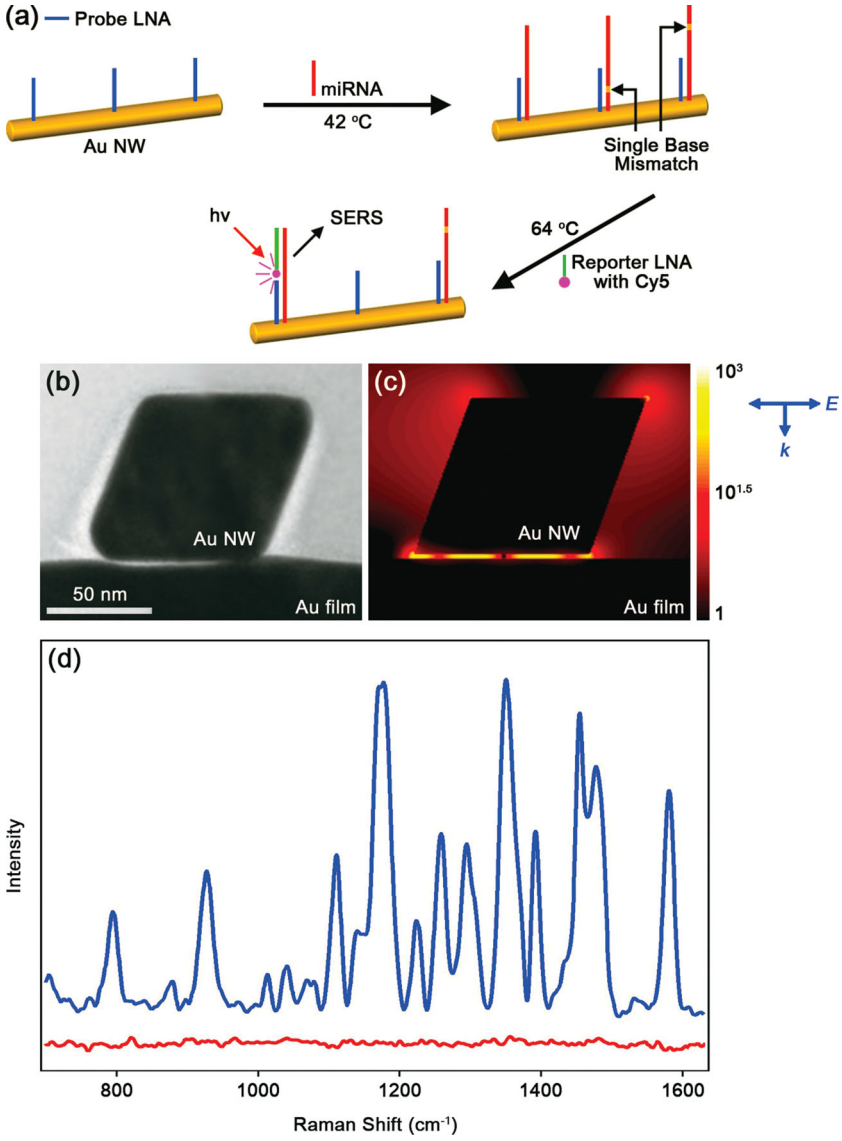

Figure 1. a) Schematic representation of miRNA detection by PNI sensors worked with bi-temperature hybridization. Firstly, PNI sensor is prepared by laying down the probe LNA-modified Au NW onto Au film. Secondly, perfectly matched miRNA and single base mismatched miRNA are incubated with the PNI sensor in 42 °C. Finally, Cy5-labeled reporter LNA is incubated with the PNI sensor in 64 °C. Only in the presence of perfectly matched miRNA, sandwich hybridization of probe LNA-miRNA-reporter LNA can be formed in the PNI sensor and strong SERS signals of Cy5 can be obtained. b) Cross-sectional TEM image of the PNI sensor. c) Calculated distributions of the local electric field intensities, $|E|^2$, of PNI sensor at the excitation wavelength of 632.8 nm. The *k*- and *E*-vectors indicate the incident direction of light and the polarization direction, respectively. d) SERS spectra of Cy5 measured from PNI sensors in the presence of perfectly matched miRNA (miR206; blue spectrum) and of single base mismatched miRNA (miR206 A; red spectrum), both in 100 pM concentrations.

were modified with thiolated locked nucleic acids (LNAs) and then transferred onto a Au film by using a nanomanipulator. LNA is a modified RNA nucleotide that can offer substantially increased affinity for its complementary strand.[46] The cross-sectional transmission electron microscope (TEM) image of a PNI sensor illustrates a Au NW with a rhombic cross-section sitting on a smooth Au film (Figure 1b). Since Au NWs are single-crystalline with very well-defined facets and atomically flat surfaces, the PNI sensor provides highly reproducible as well as sensitive SERS signals at the gap between the NW and the film upon laser excitation. Distribution of the local electric field intensities, $|E|^2$, over the PNI sensor was calculated by the finite-difference time-domain (FDTD) method at an excitation wavelength of 632.8 nm (Figure 1c). The *k*- and *E*-vectors indicate the incident direction of light and the polarization direction, respectively. The gap between the Au NW and Au film was set as 4 nm. This calculation indicates that a strongly enhanced electric field is locally induced at the gap between the NW and film when the NW is illuminated by the excitation light. Maximum electric field intensity enhancement of ≈ 2500 is obtained at the sharp edge of a Au NW adjacent to a Au film.

Among more than 24, 000 miRNAs that have been currently identified,[47] many miRNAs have similar sequences, often showing SNPs. Developing detection strategies to discriminate these small but sequentially similar miRNAs has been quite challenging. To detect intact miRNAs, we adopted sandwich hybridization strategy. Although this strategy has been quite effective in detecting normal DNAs and RNAs,[38,48–51] sensitive and selective detection of miRNAs by this method can be difficult because miRNAs are short and have very similar sequences. We utilized a sandwich hybridization of probe LNA-target miRNA-reporter LNA structure for SERS detection and found that attaching the reporter LNA at higher temperature distinctly increases target selectivity, consistent with a previous report.[46] In experiments, probe LNA-modified PNI sensors were incubated with various miRNAs at 42 °C and subsequently incubated with Cy5-labeled reporter LNA at 64 °C (Figure 1a). If the target miRNAs have perfectly complementary sequences to both probe and reporter LNAs, sandwiched complexes of probe LNA-miRNA-reporter LNA can be stably formed on a PNI sensor, providing strong SERS signals of Cy5. Blue spectrum in Figure 1d shows clear and strong SERS spectra of Cy5 measured from PNI sensors for the sample of perfectly matched miR206. In contrast, when the sample only contains single base mismatched miR206 A, little signal was observed (red spectrum in Figure 1d). Both samples are in 100 pM concentrations. SERS signals of Cy5 by non-specific adsorption were hardly observed because the PNI sensors were washed with buffers several times before the measurements. The clear signal difference indicates very high specificity of this detection scheme (Figure S1 in Supporting Information).

To further evaluate the specificity, we prepared probe (Probe 1, 2, 3, and 4) and reporter LNAs (Reporter 1, 2, 3, and 4) that match four target miRNAs (miR206, let-7a, miR21, and miR96) as written in the inset of **Figure 2**a-d. We also prepared two different types of SNPs on the target miRNAs. One had a single base mismatch on the probe LNA recognition site (miRNA A) and the other had a single base

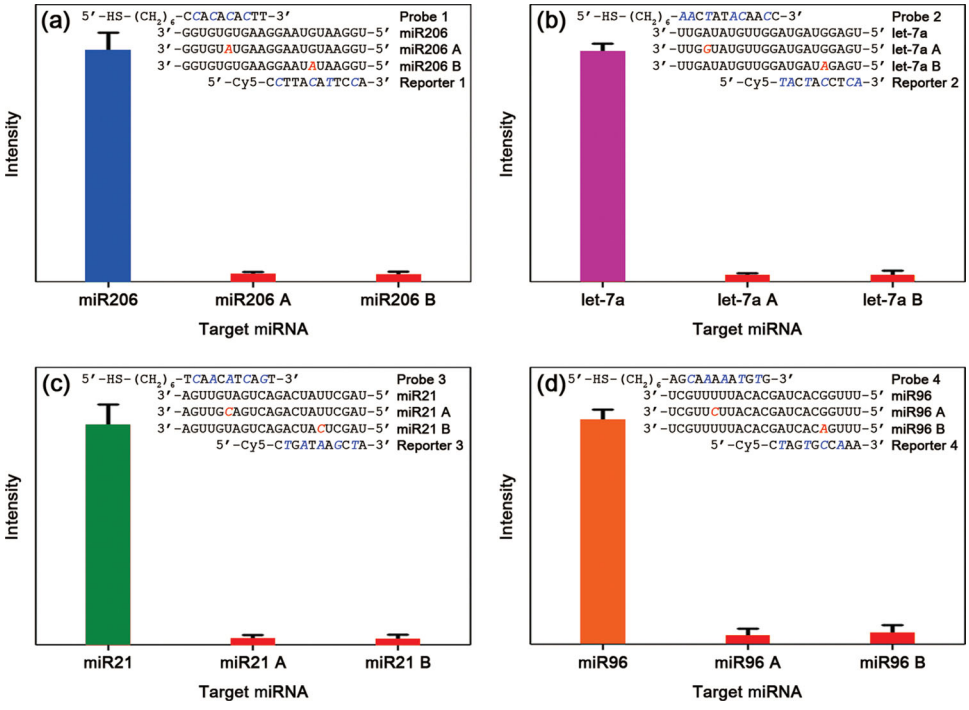

Figure 2. a–d) Plots of 1580 cm^{-1} band intensity with various target miRNAs in concentrations of 100 pM. When the target is perfectly matched miRNAs (miR206, let-7a, miR21, and miR96), strong SERS signals of Cy5 are obtained from PNI sensors. When the targets are single base mismatched miRNAs (miR206 A and B, let-7a A and B, miR21 A and B, and miR96 A and B), featureless signals are obtained. The sequences of probe (Probe 1, 2, 3, and 4) and reporter LNAs (Reporter 1, 2, 3, and 4) and target miRNAs are written in the inset of each figure. Data represent the mean plus standard deviation from ten measurements.

NANO MICRO small

mismatch on the reporter LNA recognition site (miRNA B). These were prepared for all four different miRNAs. The SERS band intensities at 1580 cm^{-1} were compared in Figure 2. Strong SERS signals of Cy5 were observed for perfectly matched miRNAs, while little SERS signal was observed in all single base mismatched miRNAs (Figure S2 in Supporting Information). All samples were in 100 pM concentrations. Additionally, we demonstrated the specificity of PNI sensor by using the purine-pyrimidine mismatched miRNAs (Figure S3 in Supporting Information). Weak SERS signals were obtained for purine-pyrimidine mismatched miRNAs, further confirming the specificity of PNI sensors with bi-temperature hybridization. Moreover, we investigated the specificity of PNI sensor by moving the position of single base mismatch in target miRNAs (Figure S4 in Supporting Information). Regardless of the position of single base mismatch in miRNAs, we can distinguish the perfectly matched miRNAs and single base mismatched miRNAs (Table S1 in Supporting Information).

2.2. Zeptomole Detection of miRNAs

While the PNI sensors can greatly enhance the SERS signal from the target molecules, the interstice size should be smaller than 10 nm for effective signal enhancement according to calculations. Normal DNAs or RNAs contain several hundreds of base pairs and are of a size of several tens of nm, which could be rather large to fit into a very small interstice (<10 nm). In this regard, the PNI sensors could be more optimal sensors for miRNAs of a very small size than for normal DNAs or RNAs of a larger size.

Figure 3a shows SERS intensity dependence on concentrations of miR206 measured from the PNI sensors. Cy5 SERS signals from reporter LNAs gradually decrease with decreasing concentrations of miR206. Impressively, the signal is still visible even at an extremely low concentration of 100 aM (the arrow-tagged one), distinct from the spectrum with no miRNA. Figure 3b shows the plots of 1580 cm^{-1} band intensities *versus* concentrations of four miRNAs. The signal shows decent linearity over a concentration range of 100 aM–100 pM. The estimated detection limit is 100 aM, corresponding to 50 zeptomole in a 500 μL hybridization volume. This detection limit is significantly lower than those of previously reported SERS-based miRNA sensors and comparable to some of the most sensitive detection methods employing various amplification reactions.[23,52–55] Also importantly, Figure 3b shows that SERS signals show a quite constant linearity with respect to logarithmic concentrations for all four miRNAs in spite of their varying degrees of GC contents. The ultra-smooth Au NW surface to which probe LNAs are attached, straightforward probe immobilization using thiol-gold bonding, and simple miRNA-LNA hybrid formation with equalized stabilities seem to collectively contribute to the observed equally enhanced and highly reproducible SERS signals for all investigated miRNAs.

The estimated false positive concentrations due to cross-hybridization (nonspecific binding) were all below the estimated detection limit (100 aM) of the PNI sensor (Figure 2 and Table S2 in Supporting Information). Observed ultra-specificity of PNI sensors for miRNA is superior to the previously reported LNA/bi-temperature based microarray method on glass surfaces.[46] For instance, the estimated nonspecific false concentration of 100 pM let-7c (let-7a A in this study) to let-7a specific probes was over 1 pM,[46] whereas it is only ≈36 aM in the present work. In addition, single base mismatches on the reporter LNA recognition sites were poorly discriminated on glass surfaces.[46] Compared to rough and rather irregular glass surfaces, atomically smooth single-crystalline Au surfaces of our PNI sensors provide highly uniform and well-aligned probe LNA molecular layers and effective subsequent hybridizations, which could contribute to exceptionally high specificity. It is also noteworthy that the observed near-perfect specificity of PNI sensors was achieved without any enzymatic reactions. While several enzymes have been successfully employed to improve the detection ability of SNPs, these methods often suffer from difficulties in optimizing enzymatic reactions.[13,56–60]

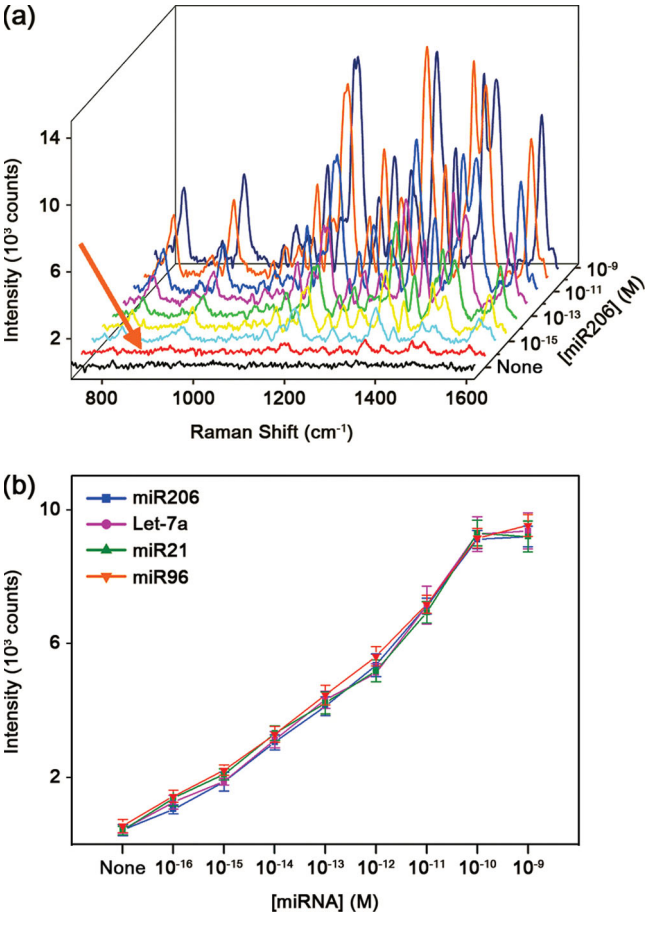

Figure 3. a) SERS spectra of Cy5 measured from PNI sensors at various concentrations of miR206. The arrow-tagged signal is for 100 aM concentration. b) Plots of 1580 cm^{-1} band intensities *versus* the concentration of four target miRNAs (miR206, let-7a, miR21, and miR96). Data represent the mean plus standard deviation from ten measurements.

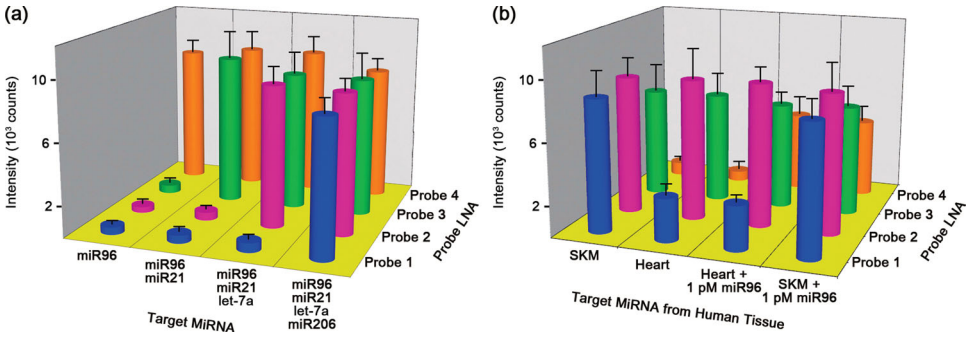

Figure 4. a) 1580 cm^{-1} band intensities measured from each PNI sensor when the sample contains one, two, three, and four kinds of target miRNAs of which concentrations are 100 pM each. b) 1580 cm^{-1} band intensities when the sample contains four kinds of total RNA extracts (SKM, heart, SKM including miR96 of 1 pM, and heart including miR96 of 1 pM). Data represent the mean plus standard deviation from ten measurements.

2.3. Multiplex Detection of miRNAs

MiRNAs, regulating gene expressions, are heavily involved in a variety of disease processes, and multiple miRNAs are often simultaneously related with disease types and stages.[7–10] For reliable miRNA-based diagnosis, many different miRNAs with diverse sequences and a wide range of concentrations must be measured simultaneously. For multiplex detection of miRNAs, we placed multiple PNI sensors in specific alignments, each of which attached with different probe LNAs. Since a single PNI sensor can detect a specific miRNA and the specific alignment of each PNI sensor provides the positional address, aligned PNI sensors can detect multiple miRNAs from miRNA mixtures (**Figure 4**a). With only miR96 in the sample, SERS signal was detected only at the PNI sensor having Probe 4. When the sample contains two, three, and four kinds of miRNAs, respectively, SERS signals were obtained only at the corresponding two, three, and four PNI sensors, respectively, indicating no cross reactivity.

Lastly, we investigated the expression patterns of four miRNAs in human tissues. Total RNA extracts from SKM and heart tissue were dissolved in a hybridization solution and applied directly to PNI sensors without any miRNA processing such as labeling or amplification. The resultant SERS signals show varying levels of miR206, let-7a, and miR21 in the total RNA extracts from human tissues with very low miR96 expression (the left half of Figure 4b and Table S2 in Supporting Information). Consistent with previous reports, let-7a is the most abundant in both SKM and heart tissues.[46,52,53,61] Calculated concentrations of let-7a in these tissues (1 μg total RNA in 500 μL sample) are over the quantitative detection range (100 pM) of the present PNI sensor. Expression patterns of miR206 and miR21 were also correlated well with previous results.[46,52,53,61] High level miR206 was detected in SKM tissues, whereas only 3.8 fM of miR206 was observed in heart tissues. The attomolar sensitivity and an exceptionally wide dynamic range of the current PNI sensor allowed simultaneous detection of highly abundant miRNAs as well as extremely low femtomolar miRNAs. To check detection accuracy for very low concentrations of miRNAs in real human samples normally containing much larger concentrations of other RNAs, a very small amount of synthetic miR96 was injected into solutions of total RNA extracts, corresponding to ≈ 0.3 parts per million. Reproducible, while somewhat reduced, concentrations of miR96 were measured (the right half of Figure 4b). Such reduction can be ascribed to the reduced activity of miRNA due to rich RNA contents in RNA extracts, suggesting the need of calibration in the human sample. Various miRNAs were also measured in the presence of human serum. Synthetic miRNAs and total RNA extracts were dissolved in 10% human serum and as-prepared PNI sensors were incubated with the miRNAs in serum at 42 °C. After second incubation with reporter LNAs at 64 °C, SERS signals were measured (Figure S7 in Supporting Information). Strong SERS signals were obtained from synthetic miRNAs even in human serum. The obtained expression levels of four miRNAs were also well-agreed with miRNA profiles of the total RNA without serum (Figure 4b). This measurement further demonstrates that PNI sensors developed here are highly reliable for multiplexed miRNA detection of the human samples.

3. Conclusion

We report highly consistent PNI sensors that allow ultra-specific and zeptomole-sensitive detection of multiple miRNAs without the need for chemical or enzymatic reactions. SERS detection of miRNA-LNA complexes formed by bi-temperature hybridization provided an impressive 100 aM (50 zeptomole) sensitivity. Compared with previously reported SERS-based miRNA sensors, this detection limit is more than two orders of magnitude lower. Furthermore, diverse single base mismatches on various miRNAs were completely discriminated. Specific miRNA detection using bi-temperature hybridization strategy was substantially improved by the present PNI sensors that feature ultra-smooth Au NW surfaces for LNA-miRNA hybridization. We also demonstrated reliable observation of expression patterns of multiple miRNAs from human tissues with multiplexed PNI sensors. PCR-like dynamic ranges (100 aM–100 pM) of our PNI sensor allowed simultaneous detection of miRNAs of a wide range of cellular concentrations. We anticipate that our approaches to measure multiple intact miRNAs with PNI sensors, featuring unprecedented combination of sensitivity and specificity, will be highly valuable for multiplexed miRNA detection and its applications such as early disease diagnosis.

NANO MICRO small

Table 1. Fitting parameters for the Drude-CP model for wavelength 400–2000 nm.

Parameter	Value
$\varepsilon\infty$	1.207
ω_p [rad s^{-1}]	1.279×10^{15}
Γ_p [rad s^{-1}]	3.561×10^{13}
ω_1, ω_2, ω_3 [rad s^{-1}]	3.805×10^{15}, 3.813×10^{15}, 4.882×10^{15}
Γ_1, Γ_2, Γ_4 [rad s^{-1}]	4.396×10^{15}, 7.674×10^{14}, 1.166×10^{16}
a_1, a_2, a_3	−2.116, 0.8750, −3.505
$\varphi1$, $\varphi2$, $\varphi3$ [rad]	−3.801, 4894, 2.774

4. Experimental Section

Materials: The thiolated probe LNA and Cy5-labeled reporter LNA were purchased from Eurogentec. The thiolated probe LNA was treated with 1 M dithiothreitol (Sigma-Aldrich) and purified by using a NAP-5 column (GE healthcare Co.). All RNA oligonucleotides were purchased from Bioneer (Daejeon, Korea). The total RNA extracts were purchased from Ambion and directly used. NaCl, $Na_3C_6H_5O_7$, and sodium dodecyl sulfate (SDS) were purchased from Sigma-Aldrich. Human serum (S7023) was purchased from Sigma-Aldrich. Phosphate buffered saline (PBS) and tween 20 were purchased from Gibco.

Numerical Calculations: In the FDTD simulation, Au was modeled with the Drude-critical points model: $\varepsilon_{(w)} = \varepsilon_\infty - \frac{\varepsilon_p^2}{\varepsilon^2 + i\omega\Gamma_p} + \sum_i A_i w_i \left(\frac{e^{i\phi_i}}{w_i - w - i\Gamma_i} + \frac{e^{-i\phi_i}}{w_i + w + i\Gamma_i} \right)$. We fit the experimentally determined dielectric function of Au in the spectral range of 400–2000 nm with three critical point terms accounting for the interband transitions.[62] The fitting parameters were set as in **Table 1**. At 632.8 nm, the complex dielectric constant of Au is −10.674 + 0.7459i. The gird size of the calculation domain was 0.25 nm and the complex-frequency-shifted perfectly matched layer was used as the absorbing boundary condition.

Preparation of PNI Sensors: Single-crystalline Au NWs were synthesized on a sapphire substrate in a horizontal quartz tube furnace system by using a previously described vapor transport method.[45] Briefly, the sapphire substrate was placed a few centimeters downstream from an alumina boat filled with an Au slug. Ar gas flowed at a rate of 100 standard cubic centimeter per minute, maintaining the chamber pressure at 1 ≈ 5 Torr. The high temperature zone of the furnace was heated to 1100 °C. Au NWs were grown on the substrate for a reaction time of 30 min. For immobilization of a probe LNA, as-grown Au NWs were incubated in the solution of 10 nM probe LNA, 3 × saline-sodium citrate (SSC; 450 mM NaCl and 45 mM $Na_3C_6H_5O_7$), and 0.04% SDS at room temperature for 12 h. The excessive probe LNA was washed with the solution of 2 × SSC and 0.1% SDS. The probe LNA-modified Au NWs were then transferred onto a Au film fabricated by electron beam assisted deposition of 10 nm Cr followed by 300 nm Au. By using a custom-built nanomanipulator with a W tip (≈100 nm diameter at the end) mounted on a 3-dimensional piezoelectric stage (Sigma-Koki), a single NW can be easily transferred on a Au film in a desired alignment, which provides multiplex sensing capability as positional addresses of the NWs.

Detection of miRNAs: Various target miRNAs in a hybridization solution (5 × SSC, 0.1% SDS, and 20 units RNase inhibitor; 500 μL) were incubated with PNI sensors at 42 °C by using a rotating hybridization incubator (Agilent) for 16 h. After hybridization, the PNI sensors were washed with a pre-warmed (42 °C) solution of 2 × SSC and 0.1% SDS. Subsequently, these sensors were treated with a mixture of reporter LNAs (10 nM of four reporter LNAs in 1 mL hybridization solution) at 64 °C for 1 h. Next, the PNI sensors were washed with PBST (PBS with 0.05% tween 20) and 0.1 ×PBS, dried under silent N_2 stream, and measured by a micro-Raman system.

Instrumentation: TEM images were taken on a JEOL JEM-2100F TEM operating at 200 kV and cross-sectional TEM specimen was prepared by a dual-beam focused ion beam (NOVA200). The micro-Raman system was home-built based on an Olympus BX41 microscope. Radiation of a He-Ne laser (Melles Griot) at 632.8 nm was used as the excitation source, and the laser was focused on an Au NW through a 100× objective (Numerical aperture = 0.7, Mitutoyo). The polarization direction of the laser was controlled by rotating a half-wave plate. SERS signals were recorded with a thermoelectrically cooled electron multiplying charge coupled device (Andor) mounted on a spectrometer with a 1200 groove per mm grating (Dongwoo Optron). Two holographic notch filters were used to remove the 633 nm light.

Supporting Information

Supporting Information is available from the Wiley Online Library or from the author.

Acknowledgements

T.K. and H.K. contributed equally to this work. H.K. is the recipient of Global Ph.D. Fellowship (NRF-2011–0030947). The work of B.K. was supported by the Korean Health Technology R&D Project (A121983) funded by the Ministry of Health & Welfare, Korea. The work of Y.J. was supported by the grant (NRF 2011–0015295) through National Research Foundation (NRF) of Korea funded by Ministry of Science, ICT, and Future Planning (MSIP). The work of B.H.C. was supported by Center for BioNano Health-Guard funded by MSIP as Global Frontier Project (H-GUARD_2013M3A6B2078950) and the KRIBB initiative Research Program.

[1] D. P Bartel, *Cell* **2004**, *116*, 281–297.
[2] E. Huntzinger, E. Izaurralde, *Nat. Rev. Genet.* **2011**, *12*, 99–110.
[3] W. P. Kloosterman, R. H. A. Plasterk, *Dev. Cell* **2006**, *11*, 441–450.
[4] C. L. Bartels, G. J. Tsongalis, *Clin. Chem.* **2009**, *55*, 623–631.
[5] J. K. Edwards, R. Pasqualini, W. Arap, G. A. Calin, *J. Cardiovasc. Transl. Res.* **2010**, *3*, 271–279.
[6] B. H. Miller, C. Wahlestedt, *Brain Res.* **2010**, *1338*, 89–99.
[7] J. Lu, G. Getz, E. A. Miska, E. Alvarez-Saavedra, J. Lamb, D. Peck, A. Sweet-Cordero, B. L. Ebet, R. H. Mak, A. A. Ferrando, J. R. Downing, T. Jacks, H. R. Horvitz, T. R. Golub, *Nature* **2005**, *435*, 834–838.

[8] S. L. Yu, H. Y. Chen, G. C. Chang, C. Y. Chen, H. W. Chen, S. Singh, C. L. Cheng, C. J. Yu, Y. C. Lee, H. S. Chen, T. J. Su, C. C. Chiang, H. N. Li, Q. S. Hong, H. Y. Su, C. C. Chen, W. J. Chen, C. C. Liu, W. K. Chan, W. J. Chen, K. C. Li, J. J. W. Chen, P. C. Yang, *Cancer Cell* **2008**, *13*, 48–57.
[9] M. F. Segura, I. Belitskaya-Levy, A. E. Rose, J. Zakrzewski, A. Gaziel, D. Hanniford, F. Darvishian, R. S. Berman, R. L. Shapiro, A. C. Pavlick, I. Osman, E. Hernando, *Clin. Cancer Res.* **2010**, *16*, 1577–1586.
[10] G. Nakajima, K. Hayashi, Y. Xi, K. Kudo, K. Uchida, K. Takasaki, M. Yamamoto, J. Ju, *Cancer Genom. Proteom.* **2006**, *3*, 317–324.
[11] P. T. Nelson, W. X. Wang, B. R. Wilfred, G. Tang, *Biochim. Biophys. Acta* **2008**, *1779*, 758–765.
[12] M. Baker, *Nat. Methods* **2010**, *7*, 687–692.
[13] C. Chen, D. A. Ridzon, A. J. Broomer, Z. Zhou, D. H. Lee, J. T. Nguyen, M. Barbisin, N. L. Xu, V. R. Mahuvakar, M. R. Andersen, K. Q. Lao, K. J. Livak, K. J. Guegler, *Nucleic Acids Res.* **2005**, *33*, e179.
[14] W. Li, K. C. Ruan, *Anal. Bioanal. Chem.* **2009**, *394*, 1117–1124.
[15] K. Tian, Z. J. He, Y. Wang, S. J. Chen, L. Q. Gu, *ACS Nano* **2013**, *7*, 3962–3969.
[16] Y. Wang, D. L. Zheng, Q. L. Tan, M. X. Wang, L. Q. Gu, *Nat. Nanotechnol.* **2011**, *6*, 668–674.
[17] P. Shah, Rorvig-A. Lund, Ben S. Chaabane, P. W. Thulstrup, H. G. Kjaergaard, E. Fron, J. Hofkens, S. W. Yang, T. Vosch, *ACS Nano* **2012**, *6*, 8803–8814.
[18] B. R. Dorvel, B. Reddy, Jr., J. Go, Duarte C. Guevara, E. Salm, M. A. Alam, R. Bashir, *ACS Nano* **2012**, *6*, 6150–6164.
[19] S. R. Ryoo, J. Lee, J. Yeo, H. K. Na, Y. K. Kim, H. Jang, J. H. Lee, S. W. Han, Y. Lee, V. N. Kim, D. H. Min, *ACS Nano* **2013**, *7*, 5882–5891.
[20] E. Kim, J. Yang, J. Park, S. Kim, N. H. Kim, J. I. Yook, J. S. Suh, S. Haam, Y. M. Huh, *ACS Nano* **2012**, *6*, 8525–8535.
[21] Z. Wang, J. Zhang, Y. Guo, X. Wu, W. Yang, L. Xu, J. Chen, F. Fu, *Biosens. Bioelectron.* **2013**, *45*, 108–113.
[22] S. Husale, H. H. J. Persson, O. Sahin, *Nature* **2009**, *462*, 1075–1078.
[23] J. L. Abell, J. M. Garren, J. D. Driskell, R. A. Tripp, Y. P. Zhao, *J. Am. Chem. Soc.* **2012**, *134*, 12889–12892.
[24] X. Zhu, X. M. Zhou, D. Xing, *Chem. Eur. J.* **2013**, *19*, 5487–5494.
[25] L. Yang, C. H. Liu, W. Ren, Z. P. Li, *ACS Appl. Mater. Interfaces* **2012**, *4*, 6450–6453.
[26] L. L. Hao, P. C. Patel, A. H. Alhasan, D. A. Giljohann, C. A. Mirkin, *Small* **2011**, *7*, 3158–3162.
[27] L. Yao, Y. Wang, S. Xu, *Chem. Commun.* **2013**, *49*, 5183–5185.
[28] Y. Cui, Q. Q. Wei, H. K. Park, C. M. Lieber, *Science* **2001**, *293*, 1289–1292.
[29] L. Y. Cao, J. S. White, J. S. Park, J. A. Schuller, B. M. Clemens, M. L. Brongersma, *Nat. Mater.* **2009**, *8*, 643–647.
[30] L. Y. Cao, P. Y. Fan, A. P. Vasudev, J. S. White, Z. F. Yu, W. S. Cai, J. A. Schuller, S. H. Fan, M. L. Brongersma, *Nano Lett.* **2010**, *10*, 439–445.
[31] L. Y. Cao, B. Nabet, J. E. Spanier, *Phys. Rev. Lett.* **2006**, *96*, 157402.
[32] H. Ko, S. Chang, V. V. Tsukruk, *ACS Nano* **2009**, *3*, 181–188.
[33] H. Ko, S. Singamaneni, V. V. Tsukruk, *Small* **2008**, *4*, 1576–1599.
[34] Y. R. Fang, H. Wei, F. Hao, P. Nordlander, H. X. Xu, *Nano Lett.* **2009**, *9*, 2049–2053.
[35] H. Wei, F. Hao, Y. Z. Huang, W. Z. Wang, P. Nordlander, H. X. Xu, *Nano Lett.* **2008**, *8*, 2497–2502.
[36] H. Wei, S. P. Zhang, X. R. Tian, H. X. Xu, *Proc. Natl. Acad. Sci.* **2013**, *110*, 4494–4499.
[37] H. J. Chen, L. Shao, Q. Li, J. F. Wang, *Chem. Soc. Rev.* **2013**, *42*, 2679–2724.
[38] T. Kang, S. M. Yoo, I. Yoon, S. Y. Lee, B. Kim, *Nano Lett.* **2010**, *10*, 1189–1193.
[39] T. Kang, S. M. Yoo, M. Kang, H. Lee, H. Kim, S. Y. Lee, B. Kim, *Lab Chip* **2012**, *12*, 3077–3081.
[40] T. Kang, S. M. Yoo, I. Yoon, S. Lee, J. Choo, S. Y. Lee, B. Kim, *Chem. Eur. J.* **2011**, *17*, 2211–2214.
[41] T. Kang, I. Yoon, J. Kim, H. Hee, B. Kim, *Chem. Eur. J.* **2010**, *16*, 1351–1355.
[42] H. Kim, T. Kang, H. Lee, H. Ryoo, S. M. Yoo, S. Y. Lee, B. Kim, *Chem. Asian J.* **2013**, *8*, 3010–3014.
[43] S. M. Yoo, T. Kang, H. Kang, H. Lee, M. Kang, S. Y. Lee, B. Kim, *Small* **2011**, *7*, 3371–3376.
[44] S. M. Yoo, T. Kang, B. Kim, S. Y. Lee, *Chem. Eur. J.* **2011**, *17*, 8657–8662.
[45] Y. Yoo, K. Seo, S. Han, K. S. K. Varadwaj, H. Y. Kim, J. H. Ryu, H. M. Lee, J. P. Ahn, H. Ihee, B. Kim, *Nano Lett.* **2010**, *10*, 432–438.
[46] J. M. Lee, Y. Jung, *Angew. Chem. Int. Ed.* **2011**, *50*, 12487–12490.
[47] A. Kozomara, Griffiths-S. Jones, *Nucleic Acids Res.* **2014**, *42*, D68-D73.
[48] M. Moskovits, *Rev. Mod. Phys.* **1985**, *57*, 783–826.
[49] L. Qin, M. J. Banholzer, J. E. Millstone, C. A. Mirkin, *Nano Lett.* **2007**, *7*, 3849–3853.
[50] J. H. Lee, J. M. Nam, K. S. Jeon, D. K. Lim, H. Kim, S. Kwon, H. Lee, Y. D. Suh, *ACS Nano* **2012**, *6*, 9574–9584.
[51] D. K. Lim, K. S. Jeon, H. M. Kim, J. M. Nam, Y. D. Suh, *Nat. Mater.* **2010**, *9*, 60–67.
[52] H. Wang, R. A. Ach, B. Curry, *RNA* **2007**, *13*, 151–159.
[53] L. A. Neely, S. Patel, J. Garver, M. Gallo, M. Hackett, S. McLaughlin, M. Nadel, J. Harris, S. Gullans, J. Rooke, *Nat. Methods* **2006**, *3*, 41–46.
[54] H. N. Wang, Vo-T. Dinh, *Small* **2011**, *7*, 3067–3074.
[55] J. D. Driskell, A. G. Seto, L. P. Jones, S. Jokela, R. A. Dluhy, Y.-P. Zhao, R. A. Tripp, *Biosens. Bioelectron.* **2008**, *24*, 917–922.
[56] R. X. Duan, X. L. Zuo, S. T. Wang, X. Y. Quan, D. L. Chen, Z. F. Chen, L. Jiang, C. H. Fan, F. Xia, *J. Am. Chem. Soc.* **2013**, *135*, 4604–4607.
[57] M. Labib, N. Khan, S. M. Ghobadloo, J. Cheng, J. P. Pezacki, M. V. Berezovski, *J. Am. Chem. Soc.* **2013**, *135*, 3027–3038.
[58] S. Fang, H. J. Lee, A. W. Wark, R. M. Corn, *J. Am. Chem. Soc.* **2006**, *128*, 14044–14046.
[59] T. Tian, H. Xiao, X. Zhang, S. Peng, X. Zhang, S. Guo, S. Wang, S. Liu, X. Zhou, C. Meyers, X. Zhou, *Chem. Commun.* **2013**, *49*, 75–77.
[60] Y. Ren, H. Deng, W. Shen, Z. Gao, *Anal. Chem.* **2013**, *85*, 4784–4789.
[61] R. A. Ach, H. Wang, B. Curry, *BMC Biotechnol.* **2008**, *8*, 69.
[62] *CRC Handbook of Chemistry and Physics* 87th ed., CRC Press, Boca Raton, FL **2006**.

Received: January 20, 2014
Revised: May 26, 2014
Published online: June 26, 2014

